Supplemental Material

Even denominator fractional quantum Hall states in the zeroth Landau level of monolayer-like band of ABA trilayer graphene

Tanima Chanda[1†], Simrandeep Kaur[1†], Harsimran Singh[1], Kenji Watanabe[2], Takashi Taniguchi[3], Manish Jain[1], Udit Khanna[4], Ajit C. Balram[5,6], Aveek Bid[1*]

[1]*Department of Physics, Indian Institute of Science, Bangalore 560012, India*

[2]*Research Center for Electronic and Optical Materials, National Institute for Materials Science, 1-1 Namiki, Tsukuba 305-0044, Japan*

[3]*Research Center for Materials Nanoarchitectonics, National Institute for Materials Science, 1-1 Namiki, Tsukuba 305-0044, Japan*

[4]*Theoretical Physics Division, Physical Research Laboratory, Navrangpura, Ahmedabad-380009, India*

[5]*Institute of Mathematical Sciences, CIT Campus, Chennai 600113, India*

[6]*Homi Bhabha National Institute, Training School Complex, Anushaktinagar, Mumbai 400094, India*

[†]*These authors contributed equally*

CONTENTS

* aveek@iisc.ac.in

SUPPLEMENTARY NOTE 1: DEVICE FABRICATION AND CHARACTERIZATION.

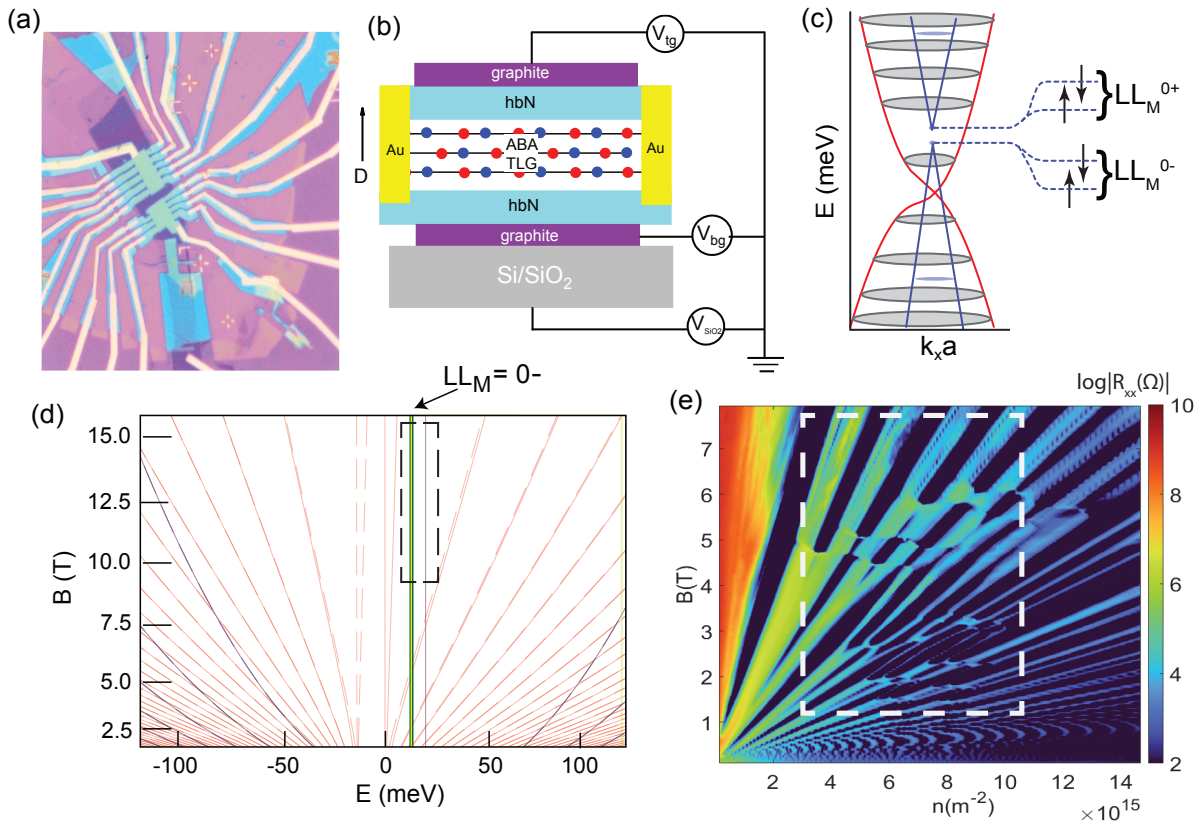

Supplementary Figure 1. **Device Schematics and characterization.** (a) Optical image of the device. (b) Device schematic showing the various gate configurations used in the measurements. The top and bottom gates were used to control the vertical displacement field D and the carrier density n across the sample with SiO_2/Si back gate used to dope the contacts. (c) Calculated band structure of Bernal-stacked trilayer graphene at $D = 0$ V/nm. The dashed line marks the $N = 0$ LLs of the MLL band, the focus of this study. (d) Calculated LL spectrum as a function of energy E and magnetic field B for $D = 0$ V/nm. The blue lines are the MLL LLs, while the red lines are the BLL LLs. Solid and dotted lines mark the LLs from the K and K'-valleys. The solid green line marks the $LL_M^{0-} \uparrow$ and $LL_M^{0-} \downarrow$ monolayer-like LLs, which host the fractional quantum Hall (FQH) states probed in this study. (e) Contour plot of R_{xx} in log scale as a function of number density and magnetic field at $D = 0$ V/nm. A dashed rectangle marks the crossing of LL_M^0 LL of the MLL band with BLL LLs, corresponding to the calculated LL plot in (d).

Bernal-stacked trilayer graphene (TLG), hBN, and graphite flakes are mechanically exfoliated on 280 nm thick SiO_2 substrate. We used optical contrast and Raman spectroscopy [1, 2] to identify ABA TLG flakes. We have fabricated heterostructure using the standard dry pickup and transfer

technique. We defined 1-D metallic contacts on the heterostructure using e-beam lithography followed by reactive ion etching using CHF_3/O_2 gas and Cr/Pd/Au thermal deposition [3, 4]. The device was then etched into a Hall bar shape (**Supplementary Figure 1**(a)). To prevent the formation of p-n junctions, we dope the graphene contacts extended out of the device using SiO_2/Si back gate.

A device schematic with different gate configurations is shown in **Supplementary Figure 1**(b). We used a dual-gate configuration to tune the vertical displacement field $D = [(C_{bg}V_{bg} - C_{tg}V_{tg})/2\epsilon_0]$ and carrier density $n = [(C_{bg}V_{bg} + C_{tg}V_{tg})/e]$ across the sample independently. Here, C_{bg} and C_{tg} represent the back-gate and top-gate capacitance, respectively. V_{bg} and V_{tg} are the back-gate and top-gate voltages. The gate capacitance is estimated from quantum Hall measurements.

Supplementary Figure 1(c) shows the calculated band structure of ABA TLG at $D = 0$ V/nm. It can be decomposed into two independent sectors – a linearly dispersing monolayer-like (MLL) band (blue solid line) and a massive bilayer-like (BLL) band (red solid line). Dashed lines mark the $LL_M^{0\pm}$ LLs formed in the MLL band at a finite perpendicular magnetic field B. Here 0 is the orbital index, and $\pm$ is the valley index of the LL. In this study, we have focused on LL_M^{0+} LL. The LLs arising from the BLL band are shown as gray ellipses.

Supplementary Figure 1(d) shows the simulated LL spectrum as a function of energy and magnetic field at $D = 0$ V/nm. Here, red lines mark the LLs from the BLL band, and blue lines mark the LLs from the MLL band. The green solid line highlights the crossing of LL_M^{0-} LL of the MLL band with several BLL LLs. **Supplementary Figure 1**(e) shows the contour plot of R_{xx} as a function of magnetic field and number density. The dashed rectangle marks the crossing region of LL_M^0 LL of the MLL band with multiple BLL LLs, confirming the system to be ABA trilayer graphene.

SUPPLEMENTARY NOTE 2: EVOLUTION OF DAUGHTER STATES WITH DISPLACEMENT FIELD.

Supplementary Figure 2(a) and **Supplementary Figure 2**(b) show the line plots of R_{xx} versus ν for different values of D in the vicinity of $\nu = 2 + 1/2$ and $\nu = 3 + 1/2$, measured at $B = 12$ T.

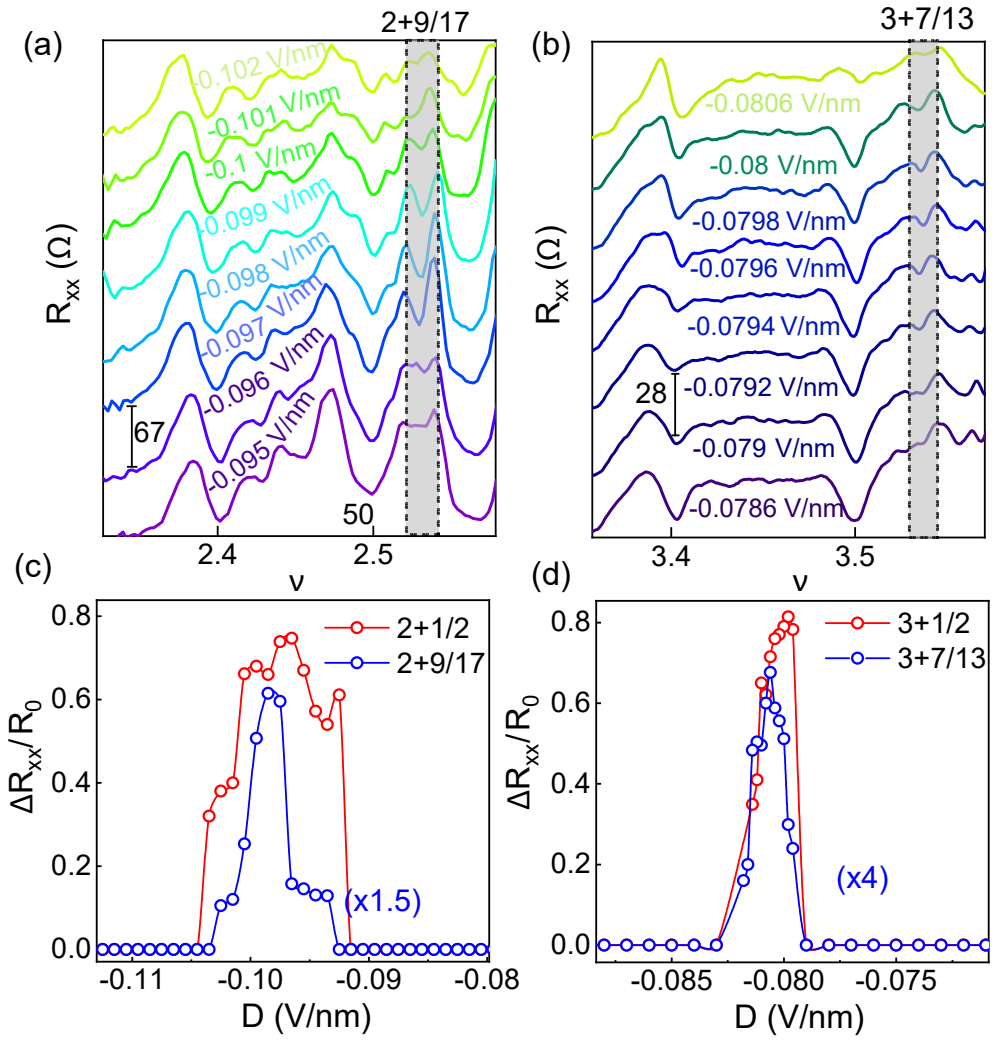

Supplementary Figure 2. Evolution of daughter states with displacement field. Plot of R_{xx} as a function of ν at different values of D in the vicinity of (a) $\nu = 2 + 1/2$, and (b). The data is taken at $B = 12$ T. The Shaded region marks the behavior of daughter states with D. (c) and (d) plots of normalized dip ($\Delta R_{xx}/R_0$) as a function of D at $\nu = 2 + 1/2, 2 + 9/17$ and $\nu = 3 + 1/2, 3 + 7/13$ respectively.

The shaded region marks the evolution of daughter states at $\nu = 2 + 9/17$ and $\nu = 3 + 7/13$ with D. Minima of R_{xx} at these fraction fillings survives over a narrow range of D: $0.095 < |D| < 0.102$ V/nm for $\nu = 2 + 9/17$ and $0.079 < |D| < 0.082$ V/nm for $\nu = 3 + 7/13$. It vanishes beyond this range of D.

To confirm these observations, we calculated normalized dips in the longitudinal resistance, $\Delta R_{xx}/R_0$, (see Supplementary Note 4) for even-denominator states at $\nu = 2 + 1/2, 3 + 1/2$ and their corresponding daughter states at $\nu = 2 + 9/17, 3 + 7/13$. **Supplementary Figure 2**(c)

and **Supplementary Figure 2**(d) show the plots of $\Delta R_{xx}/R_0$ as a function of D for FQHs at $\nu = 2 + 1/2, 2 + 9/17$ and $\nu = 3 + 1/2, 3 + 7/13$ respectively. These plots establish that the daughter state at $3 + 7/13$ $(2 + 9/17)$ appears over the same range of D as the even-denominator FQHS $\nu = 7/2$ $(\nu = 5/2)$.

SUPPLEMENTARY NOTE 3: DEPENDENCE OF $\nu = 2 + 1/2$ ON D.

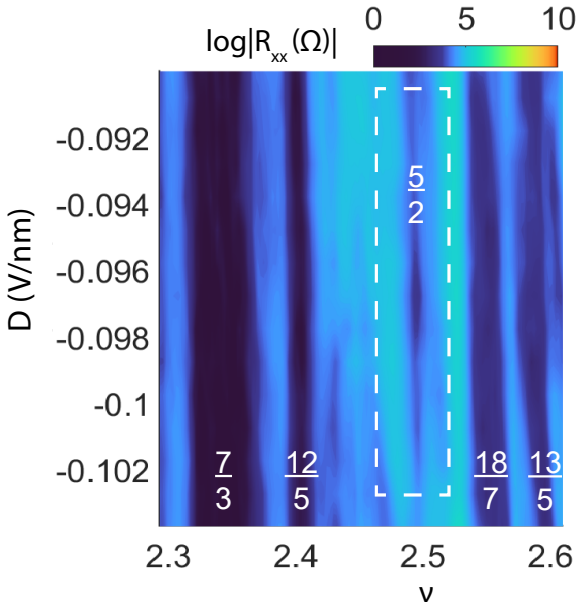

Supplementary Figure 3. Evolution of $\nu = 2 + 1/2$ state with D. Contour plot of R_{xx} as a function of ν and D measured at $B = 12$ T. Here, dashed rectangle marks the region where $\nu = 2 + 1/2$ state is formed.

Supplementary Figure 3 shows the contour plot of R_{xx} as a function of ν and D measured at $B = 12$ T. The dark region corresponds to R_{xx} minima at various fractional fillings marked in the plot. The dashed rectangle highlights the evolution of $\nu = 2 + 1/2$ state with D. Notably, $\nu = 2 + 1/2$ remains robust over the range $0.092 < |D| < 0.102$ V/nm.

Comparing it with the simulated plot in Fig 2(c) of the main manuscript, we observe that the crossing responsible for the emergence of $\nu = 2 + 1/2$ state occurs between $LL_M^{0-} \uparrow$ and $LL_M^{0+} \uparrow$ LL at crossing value of $\Delta_1 = 8.29$ meV. This is in good agreement with the experimental $|D|$ values, using the conversion factor $\Delta_1 = -[(d_\perp/2\epsilon_{TLG}) \times D]e$ [5], which leads to $\Delta_1(\mathrm{meV}) = 85\ D\ (\mathrm{V/nm})$. Here, $d_\perp$=0.67 nm is the separation between the top and bottom layers of TLG, ϵ_{TLG} is the dielectric constant of the TLG, e is the electronic charge.

This conversion factor also aligns with the observed D range ($0.079 < |D| < 0.083$ V/nm) for $\nu = 3 + 1/2$ state, corresponding to $\Delta_1 = 6.7$ meV. This value matches well with the crossing point between $LL_M^{0-} \downarrow$ and $LL_M^{0+} \uparrow$ LL of Fig 2(c) of the main manuscript. This further confirms that the origin of even denominator FQHs lies in the landau level crossings of LL_M^0 LL from the monolayer-like band.

SUPPLEMENTARY NOTE 4: DEFINITION OF $\Delta R_{xx}/R_0$

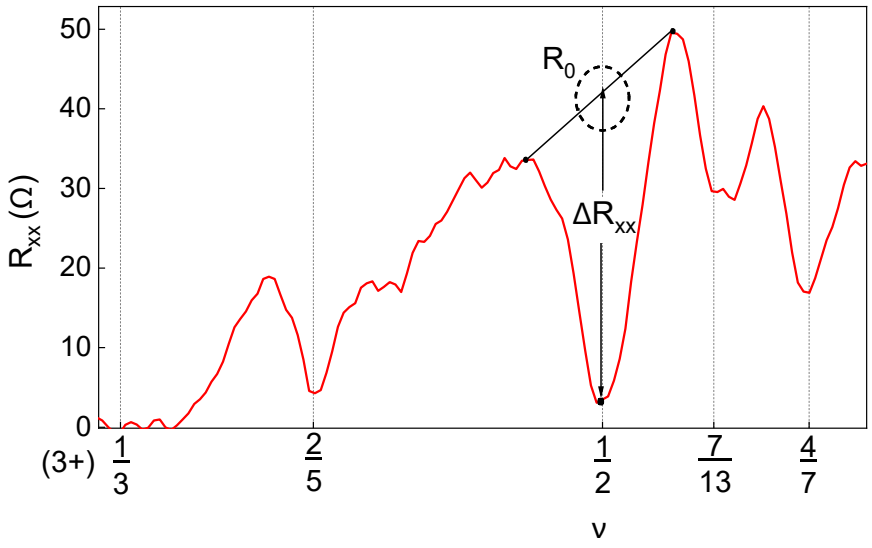

Supplementary Figure 4. Line plot of R_{xx} as a function of ν. Here, $\Delta R_{xx}/R_0$ defines the normalized dip of the even denominator FQHS.

Supplementary Figure 4 shows the line scan of R_{xx} as a function of filling factor ν in the vicinity of $\nu = 3 + 1/2$ state. This plot illustrates the method used to calculate the normalized dip of even-denominator FQHS ($\Delta R_{xx}/R_0$), which is then used to construct Fig 2(b) of the main manuscript and **Supplementary Figure 2**(c-d) of this document.

SUPPLEMENTARY NOTE 5: ENERGY GAP OF THE 4^{th} LL

Supplementary Figure 5(a) shows the plot of R_{xx} as a function of ν at different temperatures measured at $B = 13$ T and $|D| = 0.1$ V/nm in the vicinity of $LL = 4$. Arrhenius fits to data points obtained from the minima of R_{xx} at various D is shown in **Supplementary Figure 5**(b). From the slopes of these fits, we extract the values of Δ using Supplementary Equation 1.

$$R_{xx} = R_0 \exp(-\Delta/2k_B T). \qquad \text{(Supplementary Equation 1)}$$

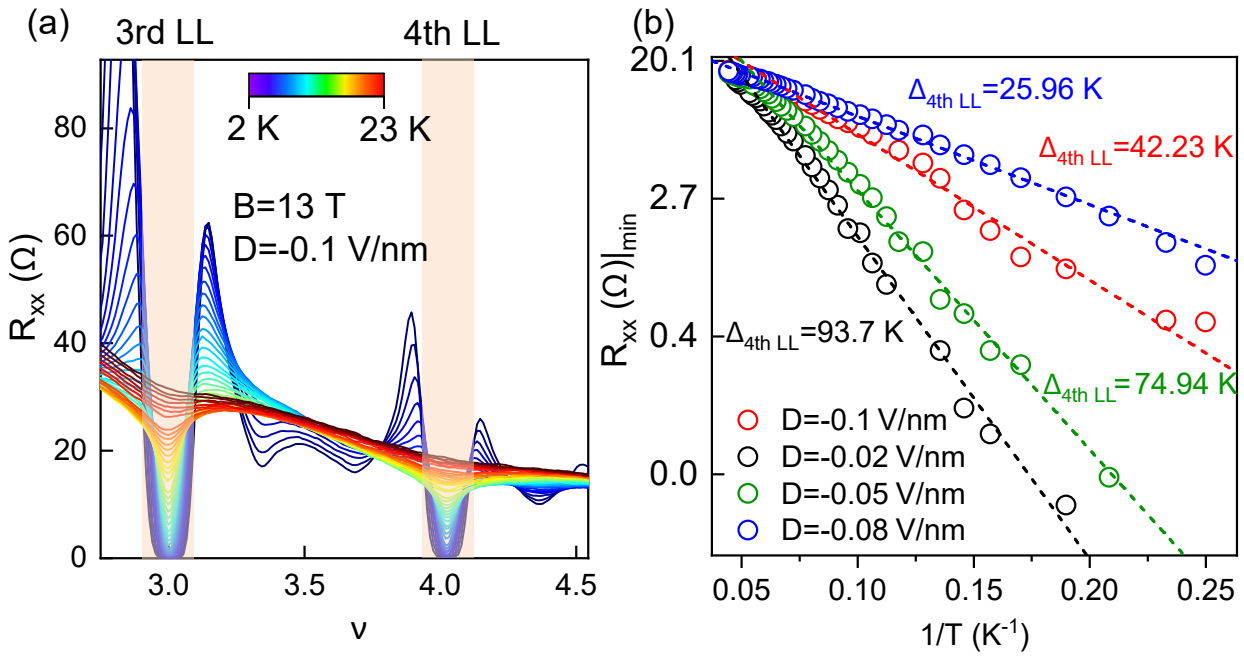

Supplementary Figure 5. **Activation gaps of the fourth LL.** (a) Line plots of R_{xx} as a function of ν at various temperatures (2 K to 23 K), measured at $B = 13$ T and $|D| = 0.1$ V/nm. (b) Arrhenius fits to R_{xx} at $|D| = -0.1$ V/nm , $|D| = 0.02$ V/nm, $|D| = 0.0$ V/nm and $|D| = 0.08$ V/nm.

SUPPLEMENTARY NOTE 6: DETAILS OF SIMULATIONS.

We have calculated the Landau spectrum at $B = 12$ T using the tight-binding model based on the Slonczewski-Weiss-McClure parametrization of tight binding model [6–8]. This model consist of six parameters $\{\gamma_0,\gamma_1,\ldots,\gamma_5\}$, which represent hopping from

$$A_i \leftrightarrow B_i : \gamma_0, B_{1/3} \leftrightarrow A_2 : \gamma_1 \qquad \text{(Supplementary Equation 2a)}$$

$$A_1 \leftrightarrow A_3 : \frac{1}{2}\gamma_2, A_{1/3} \leftrightarrow B_2 : \gamma_3 \qquad \text{(Supplementary Equation 2b)}$$

$$(A/B)_{1/3} \leftrightarrow (A/B)_2 : -\gamma_4, B_1 \leftrightarrow B_3 : \frac{1}{2}\gamma_5 \qquad \text{(Supplementary Equation 2c)}$$

where A(B) represents sublattice and index i represents layer $1\ldots3$. There is an additional parameter δ which is there to take the on-site potential for sites on top of each other (B_1, B_3, and A_2)

into account. Hamiltonian of this system in basis $\{ A_1, B_1, A_2, B_2, A_3, B_3\}$ can be written as

$$H_0 = \begin{pmatrix} 0 & \gamma_0 t_{\mathbf{k}}^* & \gamma_4 t_{\mathbf{k}}^* & \gamma_3 t_{\mathbf{k}} & \gamma_2/2 & 0 \\ \gamma_0 t_{\mathbf{k}} & \delta & \gamma_1 & \gamma_4 t_{\mathbf{k}}^* & 0 & \gamma_5/2 \\ \gamma_4 t_{\mathbf{k}} & \gamma_1 & \delta & \gamma_0 t_{\mathbf{k}}^* & \gamma_4 t_{\mathbf{k}} & \gamma_1 \\ \gamma_3 t_{\mathbf{k}}^* & \gamma_4 t_{\mathbf{k}} & \gamma_0 t_{\mathbf{k}} & 0 & \gamma_3 t_{\mathbf{k}}^* & \gamma_4 t_{\mathbf{k}} \\ \gamma_2/2 & 0 & \gamma_4 t_{\mathbf{k}}^* & \gamma_3 t_{\mathbf{k}} & 0 & \gamma_0 t_{\mathbf{k}}^* \\ 0 & \gamma_5/2 & \gamma_1 & \gamma_4 t_{\mathbf{k}}^* & \gamma_0 t_{\mathbf{k}} & \delta \end{pmatrix} \qquad \text{(Supplementary Equation 3)}$$

where $t_{\mathbf{k}} = \sum_{j=1}^{3} e^{i\mathbf{k}.\mathbf{a}_j}$, $\mathbf{a}_0 = a(0, 1/\sqrt{3}), \mathbf{a}_{1/2} = a(\mp 1/2, -1/2\sqrt{3})$ and a=2.46 Å. The effective low-energy Hamiltonian can be constructed by expanding the above Hamiltonian near K+/K- points. Low energy Hamiltonian can then be written simply by substituting $\gamma_i t_{\mathbf{k}} \rightarrow v_i \pi$, where

$$\pi = \xi k_x + i k_y \qquad \text{(Supplementary Equation 4a)}$$

$$\hbar v_i = \frac{\sqrt{3}}{2} a \gamma_i. \qquad \text{(Supplementary Equation 4b)}$$

The perpendicular electric field can be taken into account by introducing an onsite potential for each layer $V_1 \ldots V_3$, where the effect of the external and intrinsic electric field can be described by parameters Δ_1 and Δ_2 respectively.

$$\Delta_1 = (-e)\frac{V_1 - V_2}{2}, \Delta_2 = (-e)\frac{V_1 + V_3 - 2V_2}{6} \qquad \text{(Supplementary Equation 5)}$$

Without an external electric field, Hamiltonian contains monolayer-like and bilayer-like bands completely uncoupled from each other. This can be easily seen if one shifts to basis $\{ \frac{A_1 - A_3}{\sqrt{2}}, \frac{B_1 - B_3}{\sqrt{2}}, \frac{A_1 + A_3}{\sqrt{2}}, B_2, A_2, \frac{B_1 + B_3}{\sqrt{2}} \}$, where Hamiltonian takes form

$$H_0 + H_{\Delta_2} = \begin{pmatrix} H_{slg} & 0 \\ 0 & H_{blg} \end{pmatrix} \qquad \text{(Supplementary Equation 6)}$$

and external electric field couples both the blocks.

$$H_{\Delta_1} = \begin{pmatrix} 0 & H_{ext} \\ H_{ext} & 0 \end{pmatrix}, H_{ext} = \begin{pmatrix} \Delta_1 & 0 & 0 & 0 \\ 0 & 0 & 0 & \Delta_1 \end{pmatrix} \qquad \text{(Supplementary Equation 7)}$$

where

$$H_{slg} = \begin{pmatrix} \Delta_2 - \gamma_2/2 & v_0 \pi^\dagger \\ v_0 \pi & -\gamma_5/2 + \delta + \Delta_2 \end{pmatrix} \qquad \text{(Supplementary Equation 8)}$$

and

$$H_{blg} = \begin{pmatrix} \gamma_2/2+\delta & \sqrt{2}v_3\pi & -\sqrt{2}v_4\pi^\dagger & v_0\pi^\dagger \\ \sqrt{2}v_3\pi^\dagger & -2\Delta_2 & v_0\pi & -\sqrt{2}v_4\pi \\ -\sqrt{2}v_4\pi & v_0\pi^\dagger & \delta-2\Delta_2 & \sqrt{2}\gamma_1 \\ v_0\pi & -\sqrt{2}v_4\pi^\dagger & \sqrt{2}\gamma_1 & \gamma_5/2+\delta+\Delta_2 \end{pmatrix} \quad \text{(Supplementary Equation 9)}$$

the following parameters:$\gamma_0 = 3.1$ eV, $\gamma_1 = 0.39$ eV, $\gamma_2 = -0.005$ eV, $\gamma_3 = 0.275$ eV, $\gamma_4 = 0.040$ eV, $\gamma_5 = 0.005$ eV, $\delta = 0.0108$ eV, and $\Delta_2 = 0.003$ eV. For the calculation of Landau Level spectra, we make the following substitution

$$\pi \to \pi - e(A_x + iA_y) \quad \text{(Supplementary Equation 10)}$$

We then choose the Landau gauge, where $A_x = 0, A_y = Bx$. As there is no y dependence in Hamiltonian, k_y is conserved and one can see that π operators take the form

$$\pi = \frac{-i\hbar}{l_B}(\xi\partial_x + x - k_y) \quad \text{(Supplementary Equation 11)}$$

One can see, in Landau level basis at a particular value of k_y this operator acts as a raising/lowering operator.

$$K+ : \pi|n\rangle = \frac{i\hbar}{l_B}\sqrt{2(n+1)}|n+1\rangle \quad \text{(Supplementary Equation 12a)}$$

$$K+ : \pi^\dagger|n\rangle = -\frac{i\hbar}{l_B}\sqrt{2n}|n-1\rangle \quad \text{(Supplementary Equation 12b)}$$

$$K- : \pi|n\rangle = \frac{i\hbar}{l_B}\sqrt{2n}|n-1\rangle \quad \text{(Supplementary Equation 12c)}$$

$$K- : \pi^\dagger|n\rangle = -\frac{i\hbar}{l_B}\sqrt{2(n+1)}|n+1\rangle \quad \text{(Supplementary Equation 12d)}$$

We then choose a cutoff for Landau Level basis α. Thus π operators are then replaced by $\alpha \times \alpha$ matrices. Choosing a finite cutoff will give rise to unphysical eigenvalues in the low-energy regions. These eigenvalues can be removed by filtering the eigenvalues which have large $|n\rangle$ contributions. For our calculations, we choose $\alpha = 100$.

SUPPLEMENTARY NOTE 7: THEORETICAL DISCUSSIONS.

In the main text, we conjectured that the lack of inversion symmetry in TLG introduces additional lattice-scale couplings that promote LL mixing and stabilize the even-denominator FQHS in the

regime where two LLs with different valley indices are close in energy. In this section, we discuss why this might be the case.

In an ideal (zero-width and no LL mixing) two-component n=0 LL system, where the Coulomb interaction is $SU(2)$ symmetric, and the two components are exactly degenerate (as is the case with real spins at zero Zeeman energy), at half-filling a pseudospin-singlet composite fermion Fermi sea is expected to be the ground state since it has the lowest energy among the various candidate states at ν=1/2 (see **Supplementary Table 1**) (Note that for any two-body interaction, like the Coulomb one, the Moore-Read Pfaffian [9] and its hole-conjugate, the anti-Pfaffian [10, 11], have identical energies in the thermodynamic limit.). Therefore, with an $SU(2)$ symmetric interaction like the ideal Coulomb in the n=0 LL, which is strongly repulsive at short distances, an FQHE state is unlikely to materialize at half-filling, in contrast with our experimental observations.

However, the interactions' $SU(2)$ symmetry is broken in the valley sector in graphene [12]. Lattice-scale corrections in monolayer (and bilayer) graphene reduce the symmetry of the two-body interactions down to $U(1)\times Z_2$ [13], where the $U(1)$ arises from the conservation of lattice momentum and corresponds to the conservation of the difference in the number of electrons between the two valleys, and the Z_2, which renders the interactions invariant under the exchange of the valley indices, is a manifestation of the microscopic inversion symmetry in the lattice. Despite this reduced symmetry, the separate charge conservation in each valley [imposed by the $U(1)$] rules out any LL-mixing between the two LLs with different valleys. Therefore, the interaction at and near the crossing point of two n=0 LLs with different valleys is also likely to be strongly repulsive at short distances. This expectation is in line with experiments probing the crossing of two LLs with n=0 orbital index but different valleys in bilayer graphene where no FQHS is observed at half-filling [14]. Thus, we conjecture that when two LLs come close in this system of ABA-trilayer graphene, there is an avoided level-crossing wherein at the minimal gap point and in its vicinity, LL mixing gets enhanced [the orbitals of the two bare n=0 LLs have to hybridize in a non-trivial manner to break the $U(1)$ symmetry and allow for LL mixing] which changes the effective electron-electron interaction in the lower LL of our interest. Generically, in this two-component system, all three interactions $V^{\uparrow,\uparrow}(r)$, $V^{\uparrow,\downarrow}(r) = V^{\downarrow,\uparrow}(r)$ and $V^{\downarrow,\downarrow}(r)$ [we use the notation for spins with the understanding that these refer to pseudospins with specific valley-spin combinations] will be different since Z_2 symmetry is absent and the orbitals hybridize in a complex way. In this $SU(2)$-symmetry broken setting one possibility is that the two-component Halperin-331 is

realized.

The other possibility is that in the lower LL of interest, due to LL mixing with the upper LL, the short-range part of the Coulomb repulsion is softened (analogous to what happens as one goes from the lowest LL to the second LL of GaAs), and the Moore-Read Pfaffian or the anti-Pfaffian states can be stabilized over the fully polarized CF Fermi sea in this lower LL (single-component system) of interest. On one flank of $5/2$, we observe FQHE at ν=2+9/17 which could be the Levin-Halperin daughter state [15] of either the anti-Pfaffian or the Halperin-113 [16, 17]. However, since the Halperin-113 wave function phase separates [18, 19] [although a legitimate FQHS sharing the same topological properties as Halperin-113 could be realized, no evidence for such a scenario has been presented in the literature], we surmise that the $5/2$ state likely resides in the same topological phase as the anti-Pfaffian. Furthermore, since we see a weak indication of a developing FQHS at ν=3+8/17 in the vicinity of $7/2$, and $8/17$ is a Levin-Halperin daughter of the Moore-Read state but not of Halperin-331. Moreover, the FQHSs away from half-filling at the displacement field where the half-FQHSs are the strongest fit the standard Jain sequence of one-component composite fermion states. Therefore, we suggest that the half-filled states we observe at $5/2$ and $7/2$ are single-component and hence could support non-Abelian anyons (see **Supplementary Table 1**). For completeness, we note here that an alternative mechanism for an FQHE at $8/17$, that does not rely on the Levin-Halperin daughter-state construction, was recently proposed in Ref. [20] but it is unclear if that state could be stabilized in this platform. The scenario for single-component states that we have presented is akin to what has been experimentally observed in the N=1 LL of bilayer graphene [14, 21] and in the N=0 LL of wide-quantum wells of GaAs [22]. There has also been theoretical work supporting the one-component nature of the FQHSs realized in the settings mentioned in the previous line [23–27]. Nevertheless, we cannot conclusively rule out two-component FQHSs. The different candidate FQHSs at half-filling can be unambiguously distinguished by carrying out thermal Hall measurements (see **Supplementary Table 1**).

States at $\nu=1/2$				
state	per-particle Coulomb energy	shift $\mathcal{S}$	chiral central charge c_-	nature of excitations
spin-singlet CF Fermi sea	$-0.46961(1)$ [28]	2	–	Abelian
fully polarized CF Fermi sea	$-0.4656(1)$ [28]	2	–	Abelian
Moore-Read Pfaffian	$-0.45682(3)$ [29]	3	$3/2$ [30]	non-Abelian
anti-Pfaffian	$-0.45682(3)$ [29]	-1	$-1/2$ [10, 11]	non-Abelian
Halperin-331	$-0.46325(1)$	3	2 [31, 32]	Abelian

Supplementary Table 1. Candidate states at half-filling, their per-particle Coulomb energy in the thermodynamic limit in the $n=0$ Landau level, Wen-Zee shift $\mathcal{S}$ [33] on the sphere, chiral central charge c_- and nature of their excitations (Abelian/non-Abelian) are given. The Hall viscosity η_H [34] is related to the shift as $\eta_H=(1/2)\hbar\mathcal{S}/(8\pi\ell^2)$. The thermal Hall conductance κ_{xy} is related to the chiral central charge as $\kappa_{xy}=c_-[\pi^2k_{\rm B}^2/(3h)]T$ [35] (Note that filled Landau levels make an additional integral contribution to c_-.). The thermal Hall conductance of the gapless composite fermion Fermi seas is not quantized.

[1] C. Cong, T. Yu, K. Sato, J. Shang, R. Saito, G. F. Dresselhaus, and M. S. Dresselhaus, Raman characterization of aba- and abc-stacked trilayer graphene, ACS Nano **5**, 8760 (2011).

[2] T. A. Nguyen, J.-U. Lee, D. Yoon, and H. Cheong, Excitation energy dependent raman signatures of aba- and abc-stacked few-layer graphene, Scientific Reports **4**, 4630 (2014).

[3] L. Wang, I. Meric, P. Y. Huang, Q. Gao, Y. Gao, H. Tran, T. Taniguchi, K. Watanabe, L. M. Campos, D. A. Muller, J. Guo, P. Kim, J. Hone, K. L. Shepard, and C. R. Dean, One-dimensional electrical contact to a two-dimensional material, Science **342**, 614 (2013), https://www.science.org/doi/pdf/10.1126/science.1244358.

[4] P. Tiwari, S. K. Srivastav, and A. Bid, Electric-field-tunable valley zeeman effect in bilayer graphene heterostructures: Realization of the spin-orbit valve effect, Phys. Rev. Lett. **126**, 096801 (2021).

[5] S. K. Srivastav, A. Udupa, K. Watanabe, T. Taniguchi, D. Sen, and A. Das, Electric-field-tunable edge transport in bernal-stacked trilayer graphene, Phys. Rev. Lett. **132**, 096301 (2024).

[6] D. A. Abanin, B. E. Feldman, A. Yacoby, and B. I. Halperin, Fractional and integer quantum Hall effects in the zeroth Landau level in graphene, Phys. Rev. B **88**, 115407 (2013).

[7] L. C. Campos, T. Taychatanapat, M. Serbyn, K. Surakitbovorn, K. Watanabe, T. Taniguchi, D. A. Abanin, and P. Jarillo-Herrero, Landau level splittings, phase transitions, and nonuniform charge distribution in trilayer graphene, Phys. Rev. Lett. **117**, 066601 (2016).

[8] Y. Chen, Y. Huang, Q. Li, B. Tong, G. Kuang, C. Xi, K. Watanabe, T. Taniguchi, G. Liu, Z. Zhu, L. Lu, F.-C. Zhang, Y.-H. Wu, and L. Wang, Tunable even- and odd-denominator fractional quantum hall states in trilayer graphene, Nature Communications **15**, 6236 (2024).

[9] K. Moon, H. Mori, K. Yang, S. M. Girvin, A. H. MacDonald, L. Zheng, D. Yoshioka, and S.-C. Zhang, Spontaneous interlayer coherence in double-layer quantum Hall systems: Charged vortices and kosterlitz-thouless phase transitions, Phys. Rev. B **95**, 5138 (1995).

[10] M. Levin, B. I. Halperin, and B. Rosenow, Particle-hole symmetry and the Pfaffian state, Phys. Rev. Lett. **99**, 236806 (2007).

[11] S.-S. Lee, S. Ryu, C. Nayak, and M. P. A. Fisher, Particle-hole symmetry and the $\nu = 5/2$ quantum Hall state, Phys. Rev. Lett. **99**, 236807 (2007).

[12] J. Alicea and M. P. A. Fisher, Graphene integer quantum Hall effect in the ferromagnetic and param-

agnetic regimes, Phys. Rev. B **74**, 075422 (2006).

[13] M. Kharitonov, Phase diagram for the $\nu = 0$ quantum Hall state in monolayer graphene, Phys. Rev. B **85**, 155439 (2012).

[14] K. Huang, H. Fu, D. R. Hickey, N. Alem, X. Lin, K. Watanabe, T. Taniguchi, and J. Zhu, Valley isospin controlled fractional quantum Hall states in bilayer graphene, Phys. Rev. X **12**, 031019 (2022).

[15] M. Levin and B. I. Halperin, Collective states of non-abelian quasiparticles in a magnetic field, Phys. Rev. B **79**, 205301 (2009).

[16] M. Yutushui, M. Hermanns, and D. F. Mross, Paired fermions in strong magnetic fields and daughters of even-denominator Hall plateaus, Phys. Rev. B **110**, 165402 (2024).

[17] E. Zheltonozhskii, A. Stern, and N. H. Lindner, Identifying the topological order of quantized half-filled Landau levels through their daughter states, Phys. Rev. B **110**, 245140 (2024).

[18] R. de Gail, N. Regnault, and M. O. Goerbig, Plasma picture of the fractional quantum Hall effect with internal SU(K) symmetries, Phys. Rev. B **77**, 165310 (2008).

[19] S. H. Simon and A. C. Balram, Phase separation in the putative fractional quantum Hall $\mathcal{A}$ phases, Phys. Rev. B **111**, 045102 (2025).

[20] A. C. Balram and N. Regnault, Fractional quantum Hall effect of partons and the nature of the 8/17 state in the zeroth Landau level of bilayer graphene, Phys. Rev. B **110**, L081114 (2024).

[21] R. Kumar, A. Haug, J. Kim, M. Yutushui, K. Khudiakov, V. Bhardwaj, A. Ilin, K. Watanabe, T. Taniguchi, D. F. Mross, and Y. Ronen, Quarter- and half-filled quantum Hall states and their competing interactions in bilayer graphene (2024), arXiv:2405.19405 [cond-mat.mes-hall].

[22] S. K. Singh, C. Wang, C. T. Tai, C. S. Calhoun, K. A. Villegas Rosales, P. T. Madathil, A. Gupta, K. W. Baldwin, L. N. Pfeiffer, and M. Shayegan, Topological phase transition between Jain states and daughter states of the $\nu = 1/2$ fractional quantum Hall state, Nature Physics 10.1038/s41567-024-02517-w (2024).

[23] W. Zhu, Z. Liu, F. D. M. Haldane, and D. N. Sheng, Fractional quantum Hall bilayers at half filling: Tunneling-driven non-abelian phase, Phys. Rev. B **94**, 245147 (2016).

[24] Z. Zhu, D. N. Sheng, and I. Sodemann, Widely tunable quantum phase transition from Moore-Read to composite Fermi liquid in bilayer graphene, Phys. Rev. Lett. **124**, 097604 (2020).

[25] A. C. Balram, Transitions from Abelian composite fermion to non-Abelian parton fractional quantum Hall states in the zeroth Landau level of bilayer graphene, Phys. Rev. B **105**, L121406 (2022).

[26] T. Zhao, W. N. Faugno, S. Pu, A. C. Balram, and J. K. Jain, Origin of the $\nu = 1/2$ fractional quantum

Hall effect in wide quantum wells, Phys. Rev. B **103**, 155306 (2021).

[27] A. Sharma, A. C. Balram, and J. K. Jain, Composite-fermion pairing at half-filled and quarter-filled lowest Landau level, Phys. Rev. B **109**, 035306 (2024).

[28] A. C. Balram and J. K. Jain, Fermi wave vector for the partially spin-polarized composite-fermion Fermi sea, Phys. Rev. B **96**, 235102 (2017).

[29] A. C. Balram and A. Wójs, Fractional quantum Hall effect at $\nu = 2 + 4/9$, Phys. Rev. Research **2**, 032035 (2020).

[30] G. Moore and N. Read, Nonabelions in the fractional quantum Hall effect, Nucl. Phys. B **360**, 362 (1991).

[31] X. G. Wen, Chiral Luttinger liquid and the edge excitations in the fractional quantum Hall states, Phys. Rev. B **41**, 12838 (1990).

[32] X.-G. Wen, Theory of the edge states in fractional quantum Hall effects, International Journal of Modern Physics B **06**, 1711 (1992).

[33] X. G. Wen and A. Zee, Shift and spin vector: New topological quantum numbers for the Hall fluids, Phys. Rev. Lett. **69**, 953 (1992).

[34] N. Read, Non-abelian adiabatic statistics and Hall viscosity in quantum Hall states and $p_x + ip_y$ paired superfluids, Phys. Rev. B **79**, 045308 (2009).

[35] C. L. Kane and M. P. A. Fisher, Quantized thermal transport in the fractional quantum Hall effect, Phys. Rev. B **55**, 15832 (1997).